

Using in-vivo human brain data to select diffusion MRI compartment models

Uran Ferizi^{1,2}, Torben Schneider², Eleftheria Panagiotaki¹, Gemma Nedjati-Gilani¹, Hui Zhang¹, Claudia Angela M. Wheeler-Kingshott², and Daniel C. Alexander¹
¹Centre for Medical Image Computing and Department of Computer Science, University College London, London, England, United Kingdom, ²NMR Research Unit, Queen Square MS Centre, Department of Neuroinflammation, UCL Institute of Neurology, London, England, United Kingdom

Target Audience: Clinicians and physicists working with models for in-vivo brain microstructure imaging.

Purpose: We want to determine which models of diffusion MRI are best at describing the signal from in-vivo human brain white matter, and how reproducible these results are across acquisition sessions.

Introduction: Diffusion MRI (dMRI) provides a non-invasive probe into the microstructure of biological tissue. However, it relies on a mathematical model relating tissue features to the MR signal. As the standard Diffusion Tensor (DT) model is known to break down for high diffusion weights (b-values), better descriptive models are necessary. Panagiotaki et al.¹ provide a taxonomy of models of dMRI consisting of one/two/three compartments, from other works^{2,3,4,5,6}. Compartment one, 'hindered' in 3D, can be: a *Tensor* (full DT), a *Zeppelin* (cylindrically symmetric DT) or a *Ball* (isotropic DT). Compartment two, 'restricted' in 2D but free in the other direction (anisotropic restriction) can be: a *Stick* (oriented line) or a *Cylinder* (as Stick, but with non-zero radius).

Compartment three, isotropically restricted, can be: a *Dot* (bound fluid), a *Sphere* (diffusion restricted to a non-zero radius), *Astrosticks* ('Sticks' isotropically in 3D) or *Astrocyinders* ('Cylinders' in 3D). This work¹ uses data from fixed rat brains and shows that all three compartments are necessary to explain multi b-value data. Here, we perform a similar experiment in-vivo on a human brain using an enriched, massively multi-shell High Angular Resolution Diffusion Imaging (HARDI) protocol. We find that, compared with the fixed tissue study¹, simpler three compartment models emerge, and that the ranking is robust to variations in the data sampling.

Method: Using a PGSE sequence, on a 3T Phillips scanner, and having obtained ethical approval, we scan a 31-yr old man in two separate non-stop sessions, each 4hrs long. We then repeat this protocol in eight sessions of 1hr. The protocol uses 32 45-directions shells, each randomly rotated to enhance the angular resolution, and $|G| = 55$ or 60 mT/m, $\delta = 6, 10, 15$ or 22 ms, and $\Delta = 30, 50, 70$ or 90 ms. Each shell has three $b=0$ acquisitions. There are nine 4mm thick sagittal slices, acquired with ZOOM-EPI, using a reduced field-of-view (FOV) technique¹¹. The FOV is centred on the mid-sagittal slice of the Corpus Callosum (CC), to which we assume the coherent CC fibres are perpendicular. The image size is 64×64 and the in-plane resolution $2\text{mm} \times 2\text{mm}$. After segmenting the CC, all voxels with $FA > 0.5$ and principal eigenvector $< 5^\circ$ from the assumed fibre direction were selected. With the voxels satisfying these conditions, we create a single dataset by averaging them. Fig.1 shows the full data set. We ignore any signal below the observed noise floor of 0.1, and fit 32 models (listed in Fig.2) via the open source software tool Camino⁷. The algorithm uses a non-linear Levenberg-Marquardt algorithm, with offset-Gaussian noise^{8,9}. We rank the fitted models using the Bayesian Information Criterion (BIC) to balance complexity with goodness-of-fit. We also test the stability of ranking by drawing at random half the number of samples from each dataset to generate 100 *Jackknife* datasets and refitting all the models.

Results: Fig.2's left column shows the models' BIC score for the 2x4hr dataset. Three compartment models come out best, as in Panagiotaki et al.¹. Zeppelin/Tensor hindered compartments outperform Ball, and the ranking shows a preference for Dot/Sphere over Astrosticks/Astrocyinders. Because of its simplicity, the Stick is slightly preferred by BIC over Cylinder. As in Panagiotaki et al.¹, the DT comes out as the worst model. Results from the 8x1hr data are very similar. The matrices show the uncertainty in the ranking from 2x4hr dataset (left) and 8x1hr dataset (right) assessed from the *Jackknife* sampler. Using this scanning protocol, the ranking is stable within various randomised subsets variations in both datasets. Fig.3 compares the fit of the highest and lowest ranked models with the best two-compartment model.

Conclusions: The ranking we obtain is similar to previous observations from fixed tissue¹, with minor differences. The fixed-tissue study's 9.4T pre-clinical scanner used much stronger gradients, i.e. much shorter pulses, which makes the acquisition much more sensitive to the size of smaller axons. In this study, our protocol employs higher angular resolution, which may significantly improve more complex models. Fig.3 illustrates that three compartments are necessary to capture the signal restriction. Future work will test the reproducibility of these results across other subjects, as well as include other models with, e.g., a distribution of pore sizes^{1,5,10} or fibre dispersion¹⁰.

References:

1. E. Panagiotaki, T. Schneider, B. Siow, M.G. Hall, M.F. Lythgoe, and D.C. Alexander. *Compartment models of the diffusion MR signal in brain white matter: A taxonomy and comparison.* Neuroimage 59, 2012;
2. P.J. Basser, J. Mattiello, and D. LeBihan. *MR diffusion tensor spectroscopy and imaging.* Biophysical Journal, 1994;
3. G.J. Stanisz, G.A. Wright, R.M. Henkelman, and A. Szafer. *An analytical model of restricted diffusion in bovine optic nerve.* MRM, 1997;
4. TEJ Behrens, MW Woolrich, M. Jenkinson, H. Johansen-Berg, RG Nunes, S. Clare, PM Matthews, JM Brady, and SM Smith. *Characterization and propagation of uncertainty in DW-MR imaging.* MRM, 2003.;
5. Y. Assaf, T. Blumenfeld-Katzir, Y. Yovel, and P.J. Basser. *Axcaliber: a method for measuring axon diameter distribution from diffusion MRI.* MRM, 2008.;
6. D.C. Alexander, P.L. Hubbard, M.G. Hall, E.A. Moore, M. Pito, G.J.M.Parker, and T.B. Dyrby. *Orientationally invariant indices of axon diameter and density from diffusion MRI.* NeuroImage, 2010.;
7. PA Cook, Y. Bai, S. Nedjati-Gilani, KK Seunarine, MG Hall, GJ Parker, and D.C. Alexander. *Camino: Open-source diffusion-MRI reconstruction and processing.* ISMRM, 2006.
8. D.Alexander, *In Laidlaw, D., Weickert, J. (Eds.). Visualization and Processing of Tensor Fields.* Springer Verlag.;
9. D.K. Jones and P.J. Basser. *"Squashing peanuts and smashing pumpkins": How noise distorts DW-MR data.* MRM, 2004.;
10. H. Zhang, P.L. Hubbard, G.J.M. Parker, and D.C. Alexander. *Axon diameter mapping in the presence of orientation dispersion with diffusion MRI.* NeuroImage, 2011.
11. B.J. Wilms, "Reduced field-of-view MRI using outer volume suppression for spinal cord diffusion imaging," MRM, 2007.

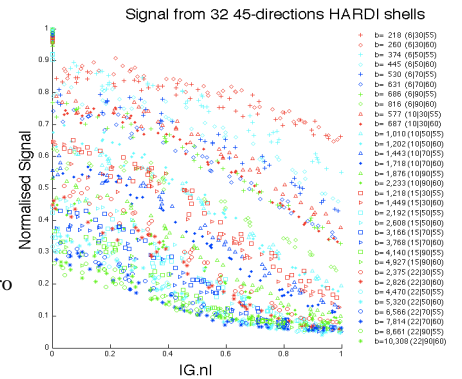


Fig.1. Total acquired signal. Legend: b-val (δ | $|G|$)

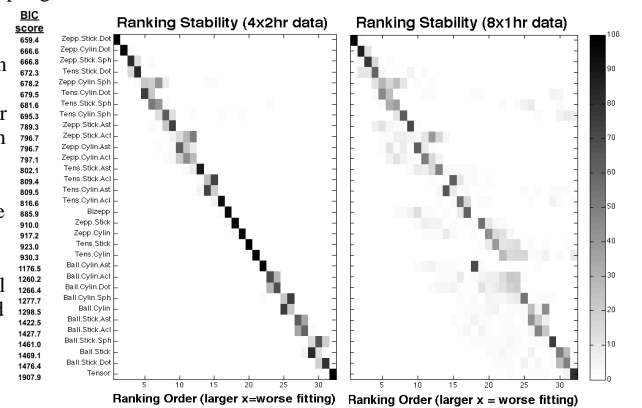


Fig.2: Each model's ranking score (left) and stability for 100 *Jackknife* samples from the 2x4hr data (left matrix) and 8x1hr data (right matrix). In the matrices, ranking frequency (x-axis) given by colour; e.g. Zeppelin-Stick-Dot comes top in 100 datasets. BIC score comes from fitting to the original 2x4hr data.

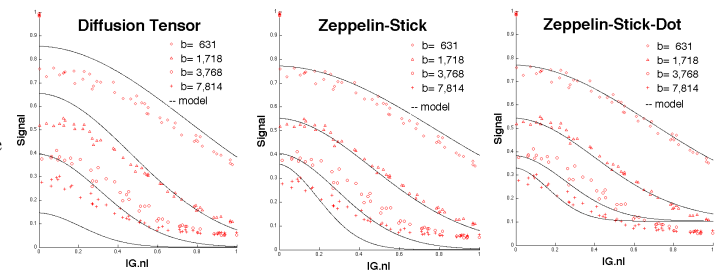


Fig.3. Synthesised signal from three representative models (solid line) with raw data (red) for 4 shells only.